

Synergistic Regulation of Pt Clusters on Porous Support by Mo and P for Robust Bifunctional Hydrogen Electrocatalysis

Yi Liu, Yi Huang, Shuqing Zhou, Yuting Yang, Lianrui Cheng, Tayirjan Taylor Isimjan,* and Xiulin Yang*



Cite This: *Inorg. Chem.* 2023, 62, 8719–8728



Read Online

ACCESS |



Metrics & More

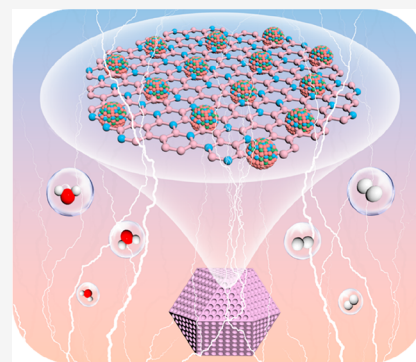


Article Recommendations



Supporting Information

ABSTRACT: Developing efficient electrocatalysts toward hydrogen oxidation and evolution reactions (HER/HOR) in alkaline electrolytes is essential for realizing renewable hydrogen technologies. Herein, we demonstrate that the introduction of dual-active species such as Mo and P (Pt/Mo,P@NC) can effectively regulate the surface electronic structure of platinum (Pt) and significantly improve the HOR/HER performance. The optimized Pt/Mo,P@NC exhibits remarkable catalytic activity, achieving a normalized exchange current density of 2.89 mA cm^{-2} and a mass activity of $2.3 \text{ mA } \mu\text{g}_{\text{Pt}}^{-1}$, which are approximately 2.2 and 13.5 times higher than those of the state-of-the-art Pt/C catalyst, respectively. Moreover, it performs an impressive HER performance with an overpotential of 23.4 mV at 10 mA cm^{-2} , which is lower than most documented alkaline electrocatalysts. Experimental results reveal that the modifying effect of Mo and P optimizes the adsorption of H and OH on Pt/Mo,P@NC, resulting in an outstanding catalytic performance. This work has significant theoretical and practical significance for developing a novel and highly efficient catalyst for bifunctional hydrogen electrocatalysis.



INTRODUCTION

Hydrogen (H_2) is generally considered a promising alternative to fossil fuels due to its clean and high gravimetric energy density properties.^{1,2} Electrochemical water electrolysis is one of the most attractive and feasible approaches to produce H_2 from abundant renewable sources.³ Hydrogen oxidation (HOR) and evolution (HER) reactions are two fundamental electrochemical processes to realize energy conversion.⁴ The former releases energy stored in chemical bonds and has essential applications in fuel cells, while the latter converts electrical energy into chemical energy at the cathode of a water electrolyzer.⁵ However, both processes require cost-effective and robust catalysts to accelerate their conversion efficiency due to the sluggish electrode kinetics. Pt and Pt-based materials are deemed as the most attractive electrocatalysts for catalytic HOR/HER, which ascribes to the appropriate adsorption/desorption energy for H_2 intermediates.⁶ Regrettably, their practical applications are severely limited by the scarcity, soaring cost, and inferior electrochemical stability of these noble metals.⁷ To overcome the dependence on noble metals, two primary approaches have been developed: developing noble-metal-free HER/HOR catalysts^{8,9} or minimizing the amount of noble metal used while maintaining a superior HOR/HER performance.^{10,11}

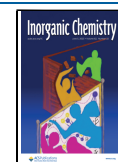
According to the acknowledged volcano plots of the exchange current and calculated hydrogen binding energy (HBE, $\Delta G_{\text{H}^*}^0$), optimal HOR electrocatalysts such as Pt present an ideal $\Delta G_{\text{H}^*}^0$ value close to zero.^{12,13} Based on the

same reaction intermediate of adsorbed hydrogen (*H), HBE is deemed as the dominant descriptor for evaluating reversible HOR and HER. Nonetheless, Pt is strongly affected by the pH.¹⁴ Yan et al. noticed a linear relationship between the HOR activity and electrolyte pH value for Pt-based catalysts.¹⁵ When the pH transforms from acidic to alkaline, the proton donor will change from H_3O^+ in H_2O , and the large presence of OH^- species makes the Volmer step the rate-determining step in alkaline HOR/HER.^{16,17} Accordingly, a bifunctional mechanism that balances both HBE and hydroxide binding energy (OHBE) has been proposed for alkaline HOR/HER electrocatalysts with better activity. For instance, Li et al. have reported a pioneering work of BCC-phased PdCu, which demonstrates that the excellent HOR activity ascribes to the synergistic interplay between OHBE and HBE.¹⁸ Our group has also proven that the synergistic optimization between HBE and OHBE determines the enhanced HOR activity of Ru/NiO@C.¹⁶

Over the past few decades, researchers have focused on modifying Pt to enhance its alkaline HOR properties.¹⁹ One approach has been to use various promoters in conjunction

Received: March 29, 2023

Published: May 23, 2023



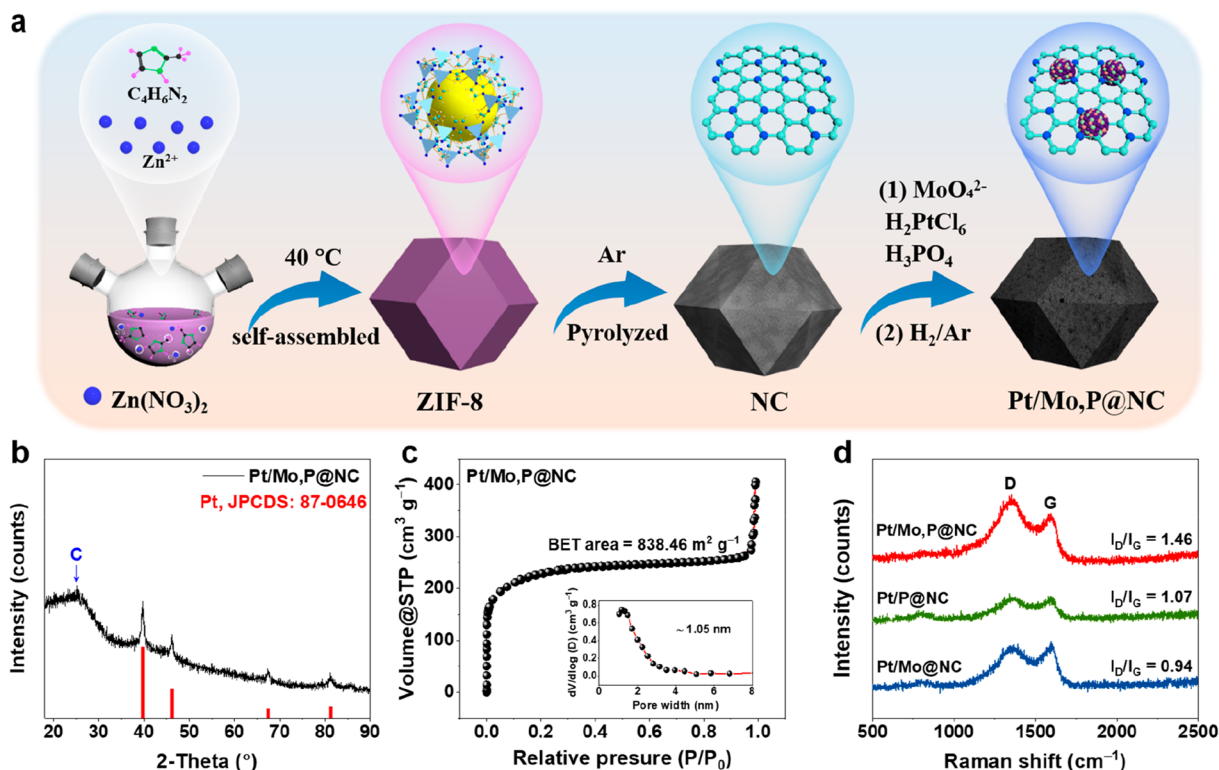


Figure 1. (a) Schematic illustration of the preparation of Pt/Mo,P@NC. (b) XRD patterns of Pt/Mo,P@NC. (c) N₂ adsorption/desorption isotherms with the corresponding pore-size distribution (inset). (d) Raman spectra of Pt/Mo,P@NC, Pt/P@NC, and Pt/Mo@NC.

with Pt to achieve a preferable HOR performance. Recent studies suggest that combining Pt with oxophilic species, such as transition metals (TMs), sulfides, and hydroxides, can alter the oxygenophilicity and electron density around the Pt site.²⁰ For example, the addition of Mo to a Pt-based catalyst has been shown to increase the mass-specific kinetic current by about 4-fold compared to an unmodified catalyst.²¹ However, the strong oxygenophilicity of TMs makes them susceptible to oxidation during hydrolysis, resulting in the formation of a Pt–M–O hybrid that impairs electron donation from the TMs to the Pt, thus limiting the potential for performance improvement. To address this issue, an effective interfacial engineering strategy that uses weakly electronegative elements such as P (2.19), B (2.04), and S (2.58) as “active auxiliaries” instead of O (3.44) can promote abundant electron transfer from TMs to Pt species.²²

With the goal of improving the HOR/HER performance, we fabricated a catalyst for oxophilic Mo and P species dual-regulated Pt clusters on a carbon support (Pt/Mo,P@NC) via a zeolitic imidazole framework (ZIF)-assisted, coadsorption, and low-temperature reduction strategy. In the Pt/Mo,P@NC hybrid, the polyhedral Mo,P@NC structures were decorated with ~1.63 nm Pt clusters. Satisfactorily, the resultant Pt/Mo,P@NC catalyst, pyrolyzed at 400 °C, exhibited an appreciable HOR performance with an exchange current density nearly 2.2 and 5.9 times higher than those of Pt/C and Pt@NC, respectively. It also displayed remarkable HER activity with overpotential as low as 23.4 mV at 10 mA cm⁻². Pt/Mo,P@NC also demonstrated excellent long-term stability, showing only a slight performance decline after 10000 s of testing. Our detailed characterizations and performance testing revealed that the exceptional HOR/HER behavior of Pt/Mo,P@NC arises from the collaborative optimization of

HBE and OHBE, along with the accessible active sites provided by the porous carbon carrier.

RESULTS AND DISCUSSION

Synthesis and Structural Characterization. The overall fabrication of Pt/Mo,P@NC involving a multistep process is schematically shown in Figure 1a. The process started with the use of ZIF-8 as a sacrificial template, followed by high-temperature annealing at 900 °C (Figure S1). Next, Pt species, Mo salts, and phosphoric acid were coadsorbed onto the template, and the resulting precursor was subjected to low-temperature reduction at 400 °C to yield Pt/Mo,P@NC. For comparison, pure Pt/Mo@NC without P modification and Pt/P@NC without Mo source were also prepared. X-ray diffraction (XRD) analysis of Pt/Mo,P@NC (Figure 1b) revealed only peaks attributed to Pt (JCPDS 87-0646) and no prominent diffraction peaks indexed to Mo species (Figure S2), indicating the presence of Mo as amorphous or very small particles.²³ Simultaneously, a broad peak of C (002) was also discovered in the sample, showing the formation of amorphous C frameworks. The N₂ adsorption/desorption isotherms (Figure 1c) showed high gas uptake at a relative pressure (P/P_0) lower than 0.02, which implied that the material was microporous.²⁴ Pt/Mo,P@NC also had a high Brunauer–Emmett–Teller surface area of 838.46 m² g⁻¹ in the $P/P_0 = 0.01–0.10$ range for the microporous samples, along with an adsorption average pore diameter of 1.05 nm. These results indicated that Pt/Mo,P@NC was microporous.²⁵ Raman spectra provided two distinct peaks of D (1354 cm⁻¹) and G (1585 cm⁻¹), corresponding to the defect/disorder and graphitization C, respectively (Figure 1d).¹⁶ The I_D/I_G value of Pt/Mo,P@NC (1.46) was much larger than those of Pt/P@NC

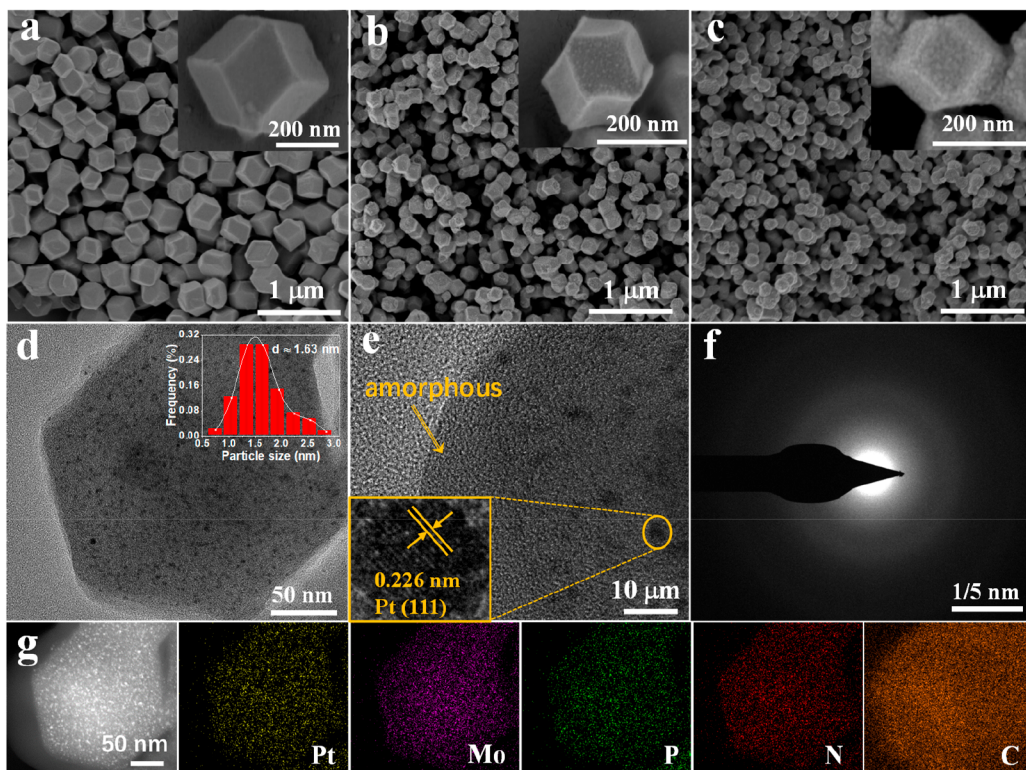


Figure 2. SEM images of (a) ZIF-8, (b) a porous NC support, and (c) Pt/Mo,P@NC. (d) TEM image of Pt/Mo,P@NC. (e) HR TEM image of Pt/Mo,P@NC. (f) SAED pattern. (g) Elemental mapping images of Pt/Mo,P@NC.

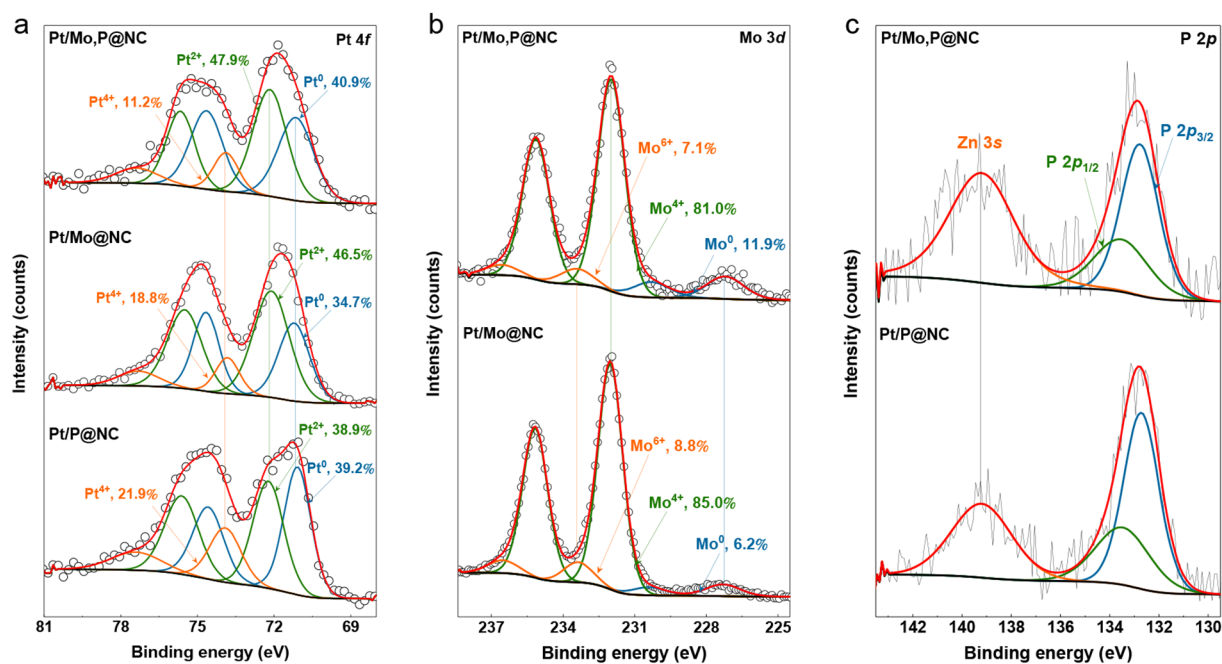


Figure 3. HR XPS spectra of (a) Pt 4f, (b) Mo 2p, and (c) P 2p in Pt/Mo,P@NC.

NC (1.07) and Pt/Mo@NC (0.94), disclosing that Pt/Mo,P@NC possessed more defect sites in the C carrier. This was attributed to the coregulation of P and Mo species, resulting in more defect sites on Pt/Mo,P@NC, which created more structural defects and adjusted the electron transport for the composite, thus exhibiting remarkable electrochemical activity.²⁶

Microstructure Analysis. The morphology of the samples was determined using scanning electron microscopy (SEM) and transmission electron microscopy (TEM). Parts a–c of Figure 2 revealed that the as-synthesized ZIF-8 was relatively homogeneous and smooth. After undergoing coadsorption and low-temperature reduction procedures, Pt/Mo,P@NC retained its initial rhombic dodecahedral shape but had a smaller particle size compared to ZIF-8. Additionally, the evaporation

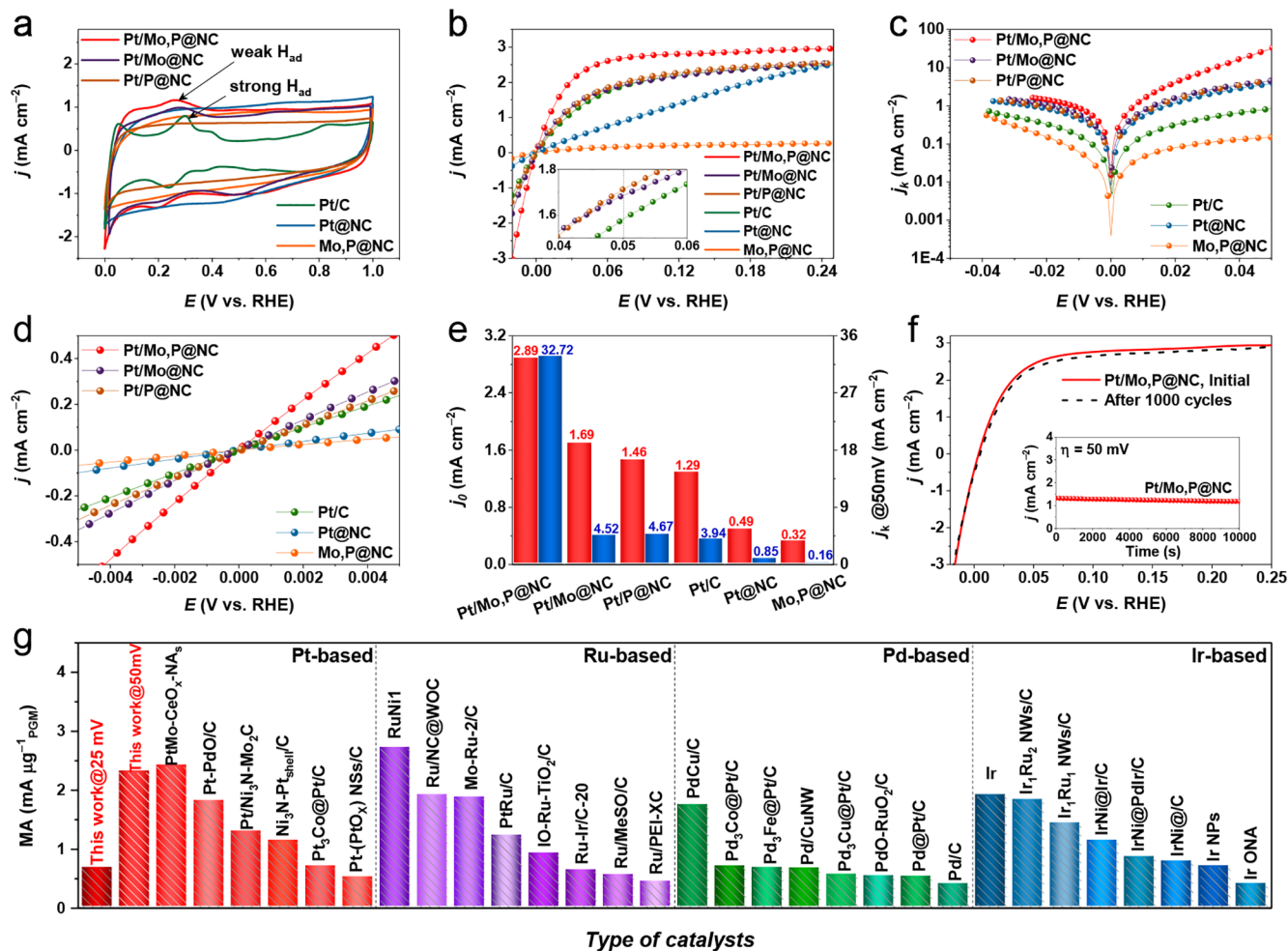


Figure 4. (a) CV curves of Pt/Mo,P@NC, Pt/Mo@NC, Pt/P@NC, Pt@NC, Mo,P@NC, and Pt/NC. (b) HOR polarization curves tested at a scan rate of 10 mV s⁻¹ and a rotating speed of 1600 rpm. (c) Tafel plots of the kinetic current density. (d) Linear fitting curves in the micropolarization region (−5 to +5 mV). (e) j_k at 50 mV and j_0 of as-made catalysts. (f) Accelerated durability test and chronoamperometric response of Pt/Mo,P@NC. (g) MA at 50 mV and different recently reported noble-based alkaline HOR electrocatalysts.

of Zn led to a rougher particle surface.²⁷ TEM observations (Figure 2d) depicted that uniform Pt clusters were dispersed uniformly in the porous C support, with an average cluster size of Pt on Pt/Mo,P@NC as small as 1.63 nm. In contrast, larger average sizes of 1.89 and 1.99 nm were found on Pt/P@NC and Pt/Mo@NC (Figure S3), respectively. These results manifested that the dual introduction of P and Mo could positively regulate the size of Pt, demonstrating a synergistic effect between P and Mo species.²⁸ Furthermore, high-resolution (HR) TEM images revealed well-resolved lattice fringes with an interplanar distance of approximately 0.226, which was identified as (111) planes of metallic Pt (Figure 2e). Meanwhile, amorphous forms were also observed, and the corresponding selected-area electron diffraction (SAED) pattern (Figure 2f) showed halo rings, which confirmed the formation of an amorphous structure.²³ The energy-dispersive X-ray spectrum (Figure S4) and elemental mapping (Figure 2g) of Pt/Mo,P@NC verified the presence of uniformly distributed Pt, Mo, P, N, and C throughout the entire architecture.

X-ray Photoelectron Spectroscopy (XPS) Analysis. XPS analysis was conducted to investigate the surface composition and electron structure in the Pt/Mo,P@NC electrocatalyst. The survey-scan XPS spectrum of Pt/Mo,P@

NC (Figure S5) confirmed the presence of Pt, Mo, P, N and C elements on the surface. The deconvoluted XPS spectrum of the C 1s regions (Figure S6) showed peaks at C=C (284.0 eV), C–C (284.8 eV), and C–O (286.0 eV), which were used as calibration criteria. The HR Pt 4f spectrum of Pt/Mo,P@NC (Figure 3a) was deconvoluted, revealing two dominant peaks at 71.5 and 74.3 eV binding energies corresponding to metallic Pt⁰. Two groups of peaks at 72.9 and 76.2 eV and at 75.2 and 78.1 eV were also observed, indicating the oxidized states of Pt²⁺ and Pt⁴⁺, respectively.²⁹ The amount of oxidized state of Pt on the Pt/Mo,P@NC surface originated from surface passivation of the Pt–O layer.³⁰ XPS results revealed that Pt/Mo,P@NC had the highest atomic percentage of 40.9% on the metallic Pt⁰ surface compared to those of Pt/Mo@NC (34.7%) and Pt/P@NC (39.2%), indicating that the comodification of Mo and P favored the generation of more active sites in Pt/Mo,P@NC.³¹ The Mo 3d XPS spectrum (Figure 3b) of Pt/Mo,P@NC and Pt/Mo@NC presented three doublets, corresponding to metallic Mo from the MoO₂ reduction under a H₂/Ar atmosphere, dominating the Mo⁴⁺ ingredient from MoO₂ and Mo⁶⁺ from further surface oxidation of MoO₂.³² The P 2p XPS spectrum (Figure 3c) of Pt/Mo,P@NC consisted of three subpeaks ascribed to P 2p_{3/2}, P 2p_{1/2}, and Zn 3s, respectively. The N 1s spectrum

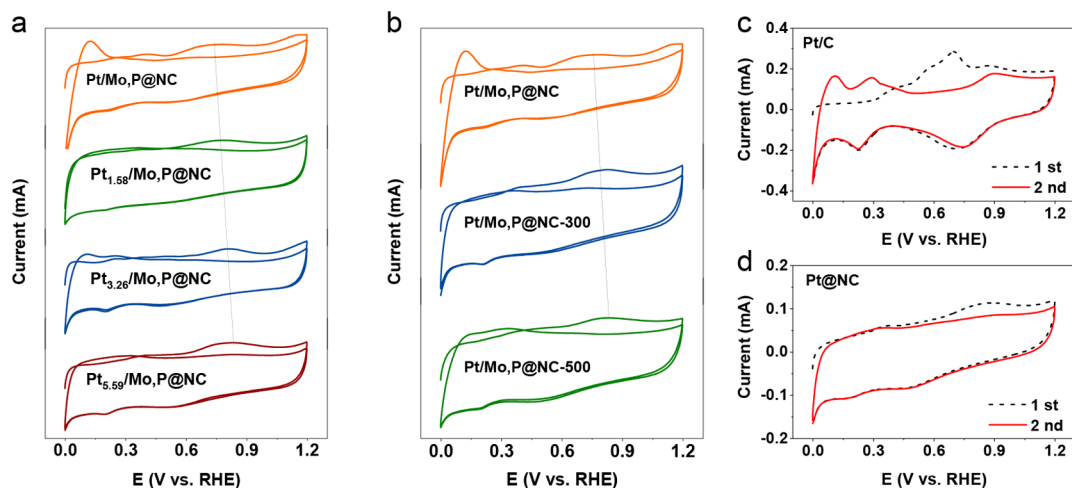


Figure 5. CO stripping curves in CO-saturated 0.1 M KOH of different studied catalysts: (a) Pt/Mo,P@NC, Pt_{1.58}/Mo, P@NC, Pt_{3.26}/Mo,P@NC, and Pt_{5.59}/Mo,P@NC; (b) Pt/Mo,P@NC at different temperatures; (c) Pt/C; (d) Pt@NC.

(Figure S7) of Pt/Mo,P@NC showed that the signals at binding energies of 396.1, 397.6, 398.8, and 400.3 eV belonged to Mo 3p, pyridinic N, pyrrolic N, and graphitic N, implying the successful doping of N, which improved the thermal/chemical stability.³³ Overall, the XPS results provided insight into the surface composition and electronic structure of the Pt/Mo,P@NC electrocatalyst, which could be useful for understanding its electrocatalytic properties.

Electrocatalytic HOR in Alkaline Electrolytes. The electrocatalytic activity of as-synthesized Pt/Mo,P@NC catalysts for HOR was investigated using a rotating disk electrode (RDE) system in a H₂-saturated 0.1 M KOH electrolyte. The measurements were conducted before reversible hydrogen electrode (RHE) calibration. All electrochemical data were conducted with *iR* corrected (Figure S8). The effect of reduction temperature on the HOR catalytic activity of Pt/Mo,P@NC was first studied, and a series of catalysts were synthesized in an H₂/Ar atmosphere. The optimal reduction temperature was found to be 400 °C, as shown in Figures S9a–c. Furthermore, the HOR activity of samples with varying Pt contents was investigated in conjunction with inductively coupled plasma emission spectrometry (Table S1). As illustrated in Figures S9d–f, the optimal Pt loading was determined to be 4.65 wt %. The catalytic performance started to increase drastically until the content was 4.65 wt % and then decreased with an increase of the Pt loading. The appearance of optimal Pt loading could be due to the Pt aggregation and unique synergy between Pt and the support.²⁸

Generally, HBE was identified as a reasonable descriptor to assess the HOR activity. The hydrogen underpotential deposition (H_{upd}) peaks in cyclic voltammetry (CV) are associated with the HBE.³⁴ In the H_{upd} region, the peak at higher potential was indexed with the stronger metal–H bond strength, while the one at lower potential corresponded to the weaker metal–H bond strength.³⁵ According to the current reports, the weaker HBE was more favorable for HOR kinetics.³⁶ As depicted in Figure 4a, the H_{upd} peak position of Pt/Mo,P@NC (0.26 V vs RHE) was more negative than that of Pt/C (0.32 V vs RHE), which was possibly due to the weakened HBE on Pt/Mo,P@NC, reflecting that Pt/Mo,P@NC had a higher HOR performance than Pt/C. In contrast,

Mo,P@NC showed an unapparent H_{upd} peak, suggesting that strong electronic interaction between Pt and Mo,P@NC can weaken the HBE.³⁷

Figure 4b exhibits the HOR polarization curves for Pt/Mo,P@NC and other comparative samples. As expected, Pt/Mo,P@NC showed the highest capacity for H₂ oxidation due to the interaction between Pt clusters and the porous C support, as well as the modulation of electronic properties in Pt clusters by the introduction of P and Mo species.³⁸ Figure S10 displays the polarization curves of Pt/Mo,P@NC tested at various rotational speeds ranging from 400 to 2500 rpm, where the plateau current increased with increasing rotating speed due to the promoted mass transport.³⁹ The corresponding Koutecky–Levich plot was calculated to be 11.87 cm² mA⁻¹ rpm^{1/2}, which verified the H₂ mass-transport-controlled process on Pt/Mo,P@NC.⁴⁰ The control experiment performed in a N₂-saturated electrolyte showed negligible anodic current throughout the entire potential range, indicating that H₂, rather than N₂, was the reactant for the HOR (Figure S11).⁴¹

Tafel plots of the kinetic current density (*j_k*) versus potential, based on the Butler–Volmer equation, are depicted in Figure 4c. Pt/Mo,P@NC demonstrated the fastest HOR kinetics due to its highest *j_k* value at random fixed potentials. The exchange current density (*j₀*) was calculated by linearly fitting the data in the micropolarization region (−5 to +5 mV). Pt/Mo,P@NC displayed remarkable intrinsic activities, as indicated by its topmost slope value, which facilitated the HOR kinetics (Figure 4d). Pt/Mo,P@NC exhibited the highest *j_k* value (6.23 mA cm⁻²) at 25 mV compared to Pt/Mo@NC (2.08 mA cm⁻²), Pt/P@NC (1.92 mA cm⁻²), and Pt/C (1.58 mA cm⁻²). Also, Pt/Mo,P@NC showed the maximal *j_k* value of 32.72 mA cm⁻² at 50 mV. Similarly, the geometric *j₀* value of Pt/Mo,P@NC was 1.7, 2.0, and 2.2 times higher than those of Pt/Mo@NC (1.69 mA cm⁻²), Pt/P@NC (1.46 mA cm⁻²), and Pt/C (1.29 mA cm⁻²), respectively, further confirming the superior HOR performance of Pt/Mo,P@NC (Figure 4e).

The long-term durability and associated capacity of Pt/Mo,P@NC for catalyzing H₂ oxidation were evaluated using chronoamperometry at $\eta = 50$ mV and polarization curves after 1000 cycles.²⁸ Interestingly, the current density presented negligible degradation at a constant potential for 10000 s, and

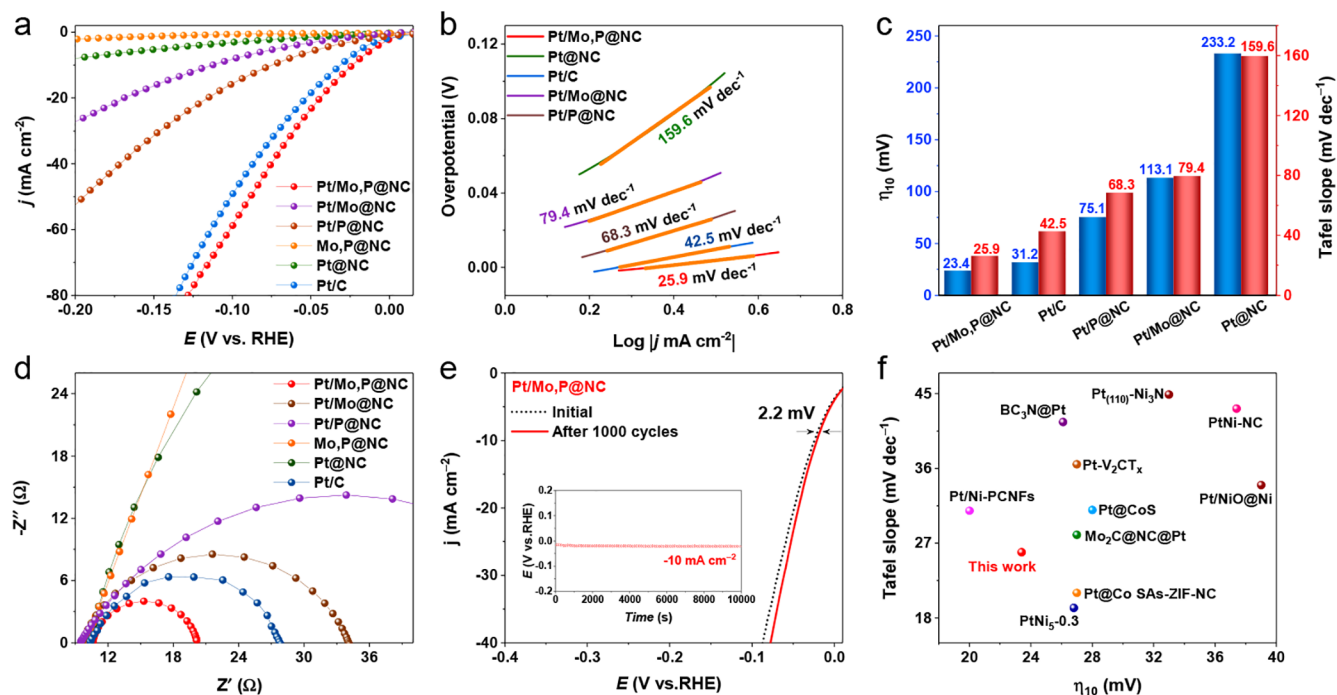


Figure 6. (a) Linear-sweep voltammetry plots of Pt/Mo,P@NC, Pt/Mo@NC, Pt/P@NC, Pt@NC, Mo,P@NC, and Pt/C. (b) Tafel plots. (c) Comparison of the overpotential at 10 mA cm^{-2} and Tafel plots of Pt/Mo,P@NC, Pt/Mo@NC, Pt/P@NC, Pt@NC, and Pt/C. (d) Nyquist plots. (e) Stability of Pt/Mo,P@NC for 1000 CV cycles in an alkaline electrolyte. (f) Comparison of the overpotential at 10 mA cm^{-2} and Tafel plots of Pt/Mo,P@NC and recently reported Pt-based catalysts.

the two polarization curves nearly overlapped after 1000 cycles, both reflecting the excellent electrochemical stability (Figure 4f). As demonstrated in Figure S12, Pt/Mo,P@NC-After HOR still retained its original morphology except for some structural collapse. Simultaneously, we discovered that the Pt/Mo,P@NC-After HOR still had Pt, Pt^{2+} , Pt^{4+} , and Mo^{4+} signals. The Mo^0 signal transformed to molybdenum oxides, which coincided with the theoretical results caused by the long-term H_2 oxidation process (Figure S13). Additionally, j_k can be normalized by the Pt loadings to acquire the mass activity (MA) values. Such an outstanding catalytic HOR performance of Pt/Mo,P@NC exceeded that of most recently reported noble-based catalysts in an alkaline environment (Figure 4g and Table S4). Besides, the HOR performance parameters of all studied catalysts are given in Table S2.

According to previous studies,³⁶ noble metals can affect the potential region for H adsorption/desorption, making it necessary to determine the electrochemical surface area (ECSA) values through CO stripping voltammetry instead of the hydrogen underpotential deposition region. As shown in Figures 5 and S14, the ECSA value of Pt/Mo,P@NC was estimated to be $83.9 \text{ m}^2 \text{ g}^{-1}$, which was higher than those of all of our studied catalysts (Table S3). A higher ECSA indicated the presence of more catalytically active sites, which facilitates better contact between the reactants and electrolyte.⁴² Besides, the HOR performance parameters of all studied catalysts are given in Table S2. Pt/Mo,P@NC showed the highest specific activity of 0.41 mA cm^{-2} .

Electrocatalytic HER in Alkaline Electrolytes. The bifunctional electrocatalytic activity of the synthesized samples was evaluated by performing HER testing in a H_2 -saturated 1 M KOH electrolyte under optimized Pt loading and reduction temperatures (Figure S15). During the measurement, high-

purity H_2 was bubbled to obtain a H_2 -saturated electrolyte, which fixed the reversible hydrogen potential and prevented the dissolution of O; this method was used widely in the literature.^{43,44} As shown in Figure 6a, Pt/Mo,P@NC exhibited superior HER activity, with a current density of 10 mA cm^{-2} at an overpotential of 23.4 mV. This performance surpassed those of Pt@NC (113.1 mV) and state-of-the-art Pt/C (31.2 mV) due to dual regulation by P and Mo. The relatively poorer performance of Pt/Mo@NC and Pt/P@NC further confirmed that the comodulation of P and Mo had a significant effect on the HER activity of Pt/Mo,P@NC.⁴⁵ Moreover, the Tafel slope of Pt/Mo,P@NC was lower ($25.9 \text{ mV decade}^{-1}$) than that of Pt/C ($42.5 \text{ mV decade}^{-1}$), suggesting that the most favorable HER kinetics was through the Volmer–Tafel mechanism (Figure 6b). A smaller Tafel slope implied that the HER rate augmented sharply with the increasing overpotential, which was advantageous for the practical HER application.^{38,46}

Figure 6c compares the overpotential at 10 mA cm^{-2} and Tafel slopes of Pt/Mo,P@NC, Pt/Mo@NC, Pt/P@NC, Pt@NC, Mo,P@NC, and Pt/NC, highlighting the optimal HER performance of Pt/Mo,P@NC. Furthermore, the electrochemical impedance spectroscopy (EIS) curves (Figure 6d) revealed the fastest HER kinetics of Pt/Mo,P@NC at the interface between the electrocatalyst and electrolyte, which was caused by its high specific surface area and the dual regulation by P and Mo species.⁴⁷ As expected, continuous cyclic tests of Pt/Mo,P@NC presented excellent durability with only 2.2 mV degradation after 1000 cycles at 10 mA cm^{-2} . Meanwhile, chronopotentiometry results showed a steady overpotential throughout the measurement at 10 mA cm^{-2} , affirming the splendid stability (Figure 6e). After multicycle CV measurement, the Pt/Mo,P@NC-After HER was basically consistent

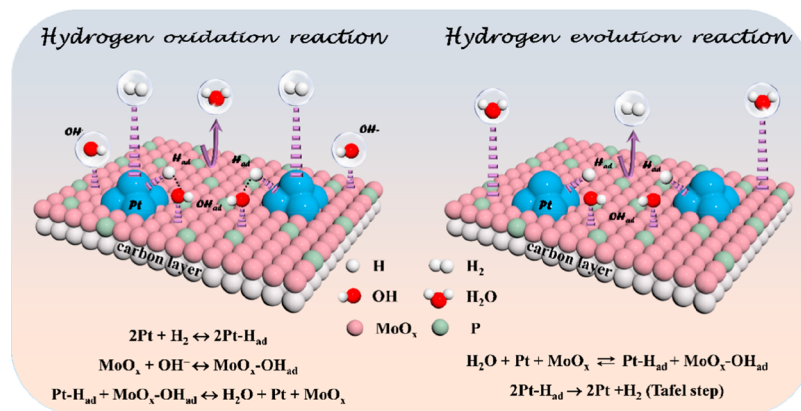


Figure 7. Mechanism diagram of Pt/Mo,P@NC for the alkaline HOR and HER processes.

with the primal morphology, but the Mo⁰ signals were all converted to molybdenum oxides (Figures S16 and S17). As illustrated in Figure 6f and Table S5, the notable HER performance of Pt/Mo,P@NC surpassed those of most reported noble-based catalysts in the alkaline environment.

Catalytic Mechanism Analysis. To gain a better understanding of the exceptional HER/HOR performance of Pt/Mo,P@NC, it was important to understand the underlying mechanisms. The CV behavior (Figure 4a) indicated that Pt/Mo,P@NC exhibited a weakened HBE, revealing that Pt/Mo,P@NC was weakly bound to H, which corresponded to H adsorption/desorption at the Pt metal sites. The performance tests showed that Pt/Mo,P@NC had the best HER/HOR activity, whereas Mo,P@NC was nearly inactive, attesting to the fact that Pt served as an active site for hydrogen adsorption (H_{ad}). Furthermore, hydroxyl adsorption (OH_{ad}) was an essential descriptor in evaluating the HOR activity. Because OH_{ad} species can accelerate the removal of a CO_{ad} intermediate on the metal surface, the CO stripping potential was directly related to the OH adsorption strength. Thus, CO stripping measurements were conducted to monitor the hydroxyl adsorption strength of the catalysts. As recorded in Figure 5a,b, the CO oxidation peak of Pt/Mo,P@NC was around 0.71 V, indicating that Pt/Mo,P@NC had the strongest OH[−] adsorption among these samples. In Figure 5c,d, the CO oxidation peaks of Pt/C and Pt@NC were at 0.73 and 0.85 V, respectively. Previous research had demonstrated that Pt bound weakly to OH_{ad} under an alkaline environment.⁴⁸ The CO stripping results suggested that the excellent HOR performance of Pt/Mo,P@NC may be due to the enhanced OH_{ad} on its surface. Luo et al. demonstrated that the introduction of Mo species made the adsorption of IrMo much stronger than that of Ir for OH, and this enhanced behavior facilitated the capture of OH on the IrMo surface, indicating that the oxyphilic Mo species can provide stronger OH adsorption sites.¹⁷

Taken together, combined CV with CO stripping experiments had proposed a bifunctional mechanism on Pt/Mo,P@NC (Figure 7). Speaking of HOR, Pt acted as a favorable adsorption site for H_{ad}, and H₂ molecules first dissociated and adsorbed on the surface of Pt metal to form H_{ad} (denoted as Pt-H_{ad}). Simultaneously, MoO_x served as an OH adsorption site to form OH_{ad} (labeled as MoO_x-OH_{ad}), and finally two intermediate species (H_{ad} and OH_{ad}) reacted to form H₂O. With respect to HER, water dissociation was a primary step that directly determined the HER activity.³⁸ Ding et al.

confirmed that Mo species can expedite the decomposition of water to form OH_{ad} and H_{ad}.⁴⁹ Based on Tafel slope analysis in Figure 6b, Pt/Mo,P@NC followed the Volmer–Tafel mechanism, and the Tafel slope of 25.9 mV dec^{−1} implied that the Tafel reaction (H_{ad} + H_{ad} = H₂) was the rate-determining step of Pt/Mo,P@NC. Specifically, water dissociation was promoted by controlling the Volmer step on the MoO_x surface to acquire OH[−] and H⁺, so that MoO_x was used to adsorb OH[−] and H⁺ was immediately adsorbed on Pt clusters. Finally, two neighboring H_{ad} on Pt sites recombined to form H₂ molecules.⁵⁰

Based on the results discussed above, it can be concluded that the improved performance of Pt/Mo,P@NC in HOR/HER can be attributed to the following combined effects: (1) The C support's extensive porous structure provided ample space for the nanoparticles' dispersion and anchoring, leading to enhanced electrical conductivity of the catalytic materials.⁵¹ (2) The metal–support interactions and interfacial engineering between Pt species and Mo,P@NC decreased charge-transfer/interfacial impedance and promoted HOR/HER kinetics.⁵² (3) The moderate HBE and OHBE on the Pt/Mo,P@NC surface synergistically facilitated the vital Volmer step.¹⁶

CONCLUSIONS

In summary, we had developed a straightforward and efficient approach to fabricate a Pt-cluster-decorated porous Mo,P@NC polyhedron. The submicron Mo,P@NC support facilitated the adsorption of Pt clusters, leading to an interaction mechanism and ultimately reduced Pt loading. Detailed characterizations, including XRD, SEM, TEM, and XPS, were conducted to analyze the crystal structure, morphology, and surface electronic structure. The optimized Pt/Mo,P@NC catalyst demonstrated excellent performance in alkaline HOR/HER, with higher mass activity and exchange current density for HOR, superior HER with lower overpotential at 10 mA cm^{−2}, and a smaller Tafel slope of 25.9 mV dec^{−1} compared to commercial Pt/C. Our systematic investigations revealed that the strong interaction between Pt clusters and the support provided more active sites and reaction centers. Furthermore, the introduction of Mo and P species synergistically optimized both H_{ad} and OH_{ad}, enhancing the HOR/HER activity and stability by imposing an electronic effect on Pt/Mo,P@NC. Overall, our approach provided a promising strategy for designing high-performance and cost-effective electrocatalysts for renewable energy conversion and storage applications.

■ ASSOCIATED CONTENT

SI Supporting Information

The Supporting Information is available free of charge at <https://pubs.acs.org/doi/10.1021/acs.inorgchem.3c01017>.

Details on the experimental method, characterization, electrochemical measurements, EIS study, and HOR and HER comparison tables (PDF)

■ AUTHOR INFORMATION

Corresponding Authors

Xiulin Yang – Guangxi Key Laboratory of Low Carbon Energy Materials, School of Chemistry and Pharmaceutical Sciences, Guangxi Normal University, Guilin 541004, China; orcid.org/0000-0003-2642-4963; Email: xlyang@gxnu.edu.cn

Tayirjan Taylor Isimjan – Saudi Arabia Basic Industries Corporation at King Abdullah University of Science and Technology, Thuwal 23955-6900, Saudi Arabia; orcid.org/0000-0003-1735-481X; Email: isimjant@sabic.com

Authors

Yi Liu – Guangxi Key Laboratory of Low Carbon Energy Materials, School of Chemistry and Pharmaceutical Sciences, Guangxi Normal University, Guilin 541004, China

Yi Huang – Guangxi Key Laboratory of Low Carbon Energy Materials, School of Chemistry and Pharmaceutical Sciences, Guangxi Normal University, Guilin 541004, China

Shuqing Zhou – Guangxi Key Laboratory of Low Carbon Energy Materials, School of Chemistry and Pharmaceutical Sciences, Guangxi Normal University, Guilin 541004, China

Yuting Yang – Guangxi Key Laboratory of Low Carbon Energy Materials, School of Chemistry and Pharmaceutical Sciences, Guangxi Normal University, Guilin 541004, China

Lianrui Cheng – Guangxi Key Laboratory of Low Carbon Energy Materials, School of Chemistry and Pharmaceutical Sciences, Guangxi Normal University, Guilin 541004, China

Complete contact information is available at:

<https://pubs.acs.org/10.1021/acs.inorgchem.3c01017>

Author Contributions

The manuscript was written through contributions of all authors. All authors have given approval to the final version of the manuscript.

Notes

The authors declare no competing financial interest.

■ ACKNOWLEDGMENTS

This work has been supported by the National Natural Science Foundation of China (No. 21965005), Natural Science Foundation of Guangxi Province (2021GXNSFAA076001), Innovation Project of Guangxi Graduate Education (YCBZ2023062), and Guangxi Technology Base and Talent Subject (GUIKEAD18126001 and GUIKE AD20297039).

■ REFERENCES

- (1) Zhan, C.; Xu, Y.; Bu, L.; Zhu, H.; Feng, Y.; Yang, T.; Zhang, Y.; Yang, Z.; Huang, B.; Shao, Q.; Huang, X. Subnanometer high-entropy alloy nanowires enable remarkable hydrogen oxidation catalysis. *Nat. Commun.* **2021**, *12*, 6261.
- (2) Jiang, H.; Sun, M.; Wu, S.; Huang, B.; Lee, C. S.; Zhang, W. Oxygen-Incorporated NiMoP Nanotube Arrays as Efficient Bifunc-

tional Electrocatalysts For Urea-Assisted Energy-Saving Hydrogen Production in Alkaline Electrolyte. *Adv. Funct. Mater.* **2021**, *31*, 2104951.

- (3) Shah, K.; Dai, R.; Mateen, M.; Hassan, Z.; Zhuang, Z.; Liu, C.; Israr, M.; Cheong, W. C.; Hu, B.; Tu, R.; Zhang, C.; Chen, X.; Peng, Q.; Chen, C.; Li, Y. Cobalt Single Atom Incorporated in Ruthenium Oxide Sphere: A Robust Bifunctional Electrocatalyst for HER and OER. *Angew. Chem., Int. Ed.* **2022**, *61*, 202114951.

- (4) Du, H.; Du, Z.; Wang, T.; Li, B.; He, S.; Wang, K.; Xie, L.; Ai, W.; Huang, W. Unlocking Interfacial Electron Transfer of Ruthenium Phosphides by Homologous Core-Shell Design toward Efficient Hydrogen Evolution and Oxidation. *Adv. Mater.* **2022**, *34*, 2204624.

- (5) Wang, M.; Yang, H.; Shi, J.; Chen, Y.; Zhou, Y.; Wang, L.; Di, S.; Zhao, X.; Zhong, J.; Cheng, T.; Zhou, W.; Li, Y. Alloying Nickel with Molybdenum Significantly Accelerates Alkaline Hydrogen Electrocatalysis. *Angew. Chem., Int. Ed.* **2021**, *60*, 5771–5777.

- (6) Huang, B.; Xiao, K.; Wei, J.-X.; Guo, X.-P.; Chen, Y.-X.; Liu, Z.-Q. In-situ precise anchoring of Pt single atoms in spinel Mn₃O₄ for highly efficient hydrogen evolution reaction. *Energy Environ. Sci.* **2022**, *15*, 4592–4600.

- (7) Zhang, D.; Zhang, Y.; Huang, Y.; Hou, C.; Wang, H.; Cai, Y.; Li, Q. Robust Oxygen Reduction Electrocatalysis Enabled by Platinum Rooted on Molybdenum Nitride Microrods. *Inorg. Chem.* **2022**, *61*, 12023–12032.

- (8) Zhao, X.; Li, X.; An, L.; Zheng, L.; Yang, J.; Wang, D. Controlling the Valence-Electron Arrangement of Nickel Active Centers for Efficient Hydrogen Oxidation Electrocatalysis. *Angew. Chem., Int. Ed.* **2022**, *61*, 202206588.

- (9) Yang, F.; Han, P.; Yao, N.; Cheng, G.; Chen, S.; Luo, W. Inter-regulated d-band centers of the Ni₃B/Ni heterostructure for boosting hydrogen electrooxidation in alkaline media. *Chem. Sci.* **2020**, *11*, 12118–12123.

- (10) Meng, G.; Cao, H.; Wei, T.; Liu, Q.; Fu, J.; Zhang, S.; Luo, J.; Liu, X. Highly dispersed Ru clusters toward an efficient and durable hydrogen oxidation reaction. *Chem. Commun.* **2022**, *58*, 11839–11842.

- (11) Zhang, X.; Li, Z.; Sun, X.; Wei, L.; Niu, H.; Chen, S.; Chen, Q.; Wang, C.; Zheng, F. Regulating the Surface Electronic Structure of RuNi Alloys for Boosting Alkaline Hydrogen Oxidation Electrocatalysis. *ACS Mater. Lett.* **2022**, *4*, 2097–2105.

- (12) Wang, J.; Dong, X.; Liu, J.; Li, W.; Roling, L. T.; Xiao, J.; Jiang, L. Ultrafine Nickel Nanoparticles Encapsulated in N-Doped Carbon Promoting Hydrogen Oxidation Reaction in Alkaline Media. *ACS Catal.* **2021**, *11*, 7422–7428.

- (13) Tian, X.; Zhao, P.; Sheng, W. Hydrogen Evolution and Oxidation: Mechanistic Studies and Material Advances. *Adv. Mater.* **2019**, *31*, 1808066.

- (14) Liu, J.; Zhang, B.; Fo, Y.; Yu, W.; Gao, J.; Cui, X.; Zhou, X.; Jiang, L. Electrochemically induced dilute gold-in-nickel nanoalloy as a highly robust electrocatalyst for alkaline hydrogen oxidation reaction. *Chem. Eng. J.* **2023**, *464*, 142692.

- (15) Zheng, J.; Sheng, W.; Zhuang, Z.; Xu, B.; Yan, Y. Universal dependence of hydrogen oxidation and evolution reaction activity of platinum-group metals on pH and hydrogen binding energy. *Sci. Adv.* **2016**, *2*, 1501602.

- (16) Yang, Y.; Huang, Y.; Zhou, S.; Liu, Y.; Shi, L.; Isimjan, T. T.; Yang, X. Delicate surface vacancies engineering of Ru doped MOF-derived Ni-NiO@C hollow microsphere superstructure to achieve outstanding hydrogen oxidation performance. *J. Energy Chem.* **2022**, *72*, 395–404.

- (17) Fu, L.; Li, Y.; Yao, N.; Yang, F.; Cheng, G.; Luo, W. IrMo Nanocatalysts for Efficient Alkaline Hydrogen Electrocatalysis. *ACS Catal.* **2020**, *10*, 7322–7327.

- (18) Qiu, Y.; Xin, L.; Li, Y.; McCrum, I. T.; Guo, F.; Ma, T.; Ren, Y.; Liu, Q.; Zhou, L.; Gu, S.; Janik, M. J.; Li, W. BCC-Phased PdCu Alloy as a Highly Active Electrocatalyst for Hydrogen Oxidation in Alkaline Electrolytes. *J. Am. Chem. Soc.* **2018**, *140*, 16580–16588.

- (19) Wang, K.; Yang, H.; Zhang, J.; Ren, G.; Cheng, T.; Xu, Y.; Huang, X. The exclusive surface and electronic effects of Ni on

promoting the activity of Pt towards alkaline hydrogen oxidation. *Nano Research* **2022**, *15*, 5865–5872.

(20) Wang, L.; Zhu, Y.; Zeng, Z.; Lin, C.; Giroux, M.; Jiang, L.; Han, Y.; Greeley, J.; Wang, C.; Jin, J. Platinum-nickel hydroxide nanocomposites for electrocatalytic reduction of water. *Nano Energy* **2017**, *31*, 456–461.

(21) Ma, M.; Li, G.; Yan, W.; Wu, Z.; Zheng, Z.; Zhang, X.; Wang, Q.; Du, G.; Liu, D.; Xie, Z.; Kuang, Q.; Zheng, L. Single-Atom Molybdenum Engineered Platinum Nanocatalyst for Boosted Alkaline Hydrogen Oxidation. *Adv. Energy Mater.* **2022**, *12*, 2103336.

(22) Wang, Y.; Zhuo, H.; Zhang, X.; Li, Y.; Yang, J.; Liu, Y.; Dai, X.; Li, M.; Zhao, H.; Cui, M.; Wang, H.; Li, J. Interfacial synergy of ultralong jagged Pt₈₅Mo₁₅-S nanowires with abundant active sites on enhanced hydrogen evolution in an alkaline solution. *J. Mater. Chem. A* **2019**, *7*, 24328–24336.

(23) Wu, J.; Hou, M.; Chen, Z.; Hao, W.; Pan, X.; Yang, H.; Cen, W.; Liu, Y.; Huang, H.; Menezes, P. W.; Kang, Z. Composition Engineering of Amorphous Nickel Boride Nanoarchitectures Enabling Highly Efficient Electrosynthesis of Hydrogen Peroxide. *Adv. Mater.* **2022**, *34*, 2202995.

(24) Wang, T.; Zhao, Y. C.; Zhang, L. M.; Cui, Y.; Zhang, C. S.; Han, B. H. Novel approach to hydroxy-group-containing porous organic polymers from bisphenol A. *Beilstein J. Org. Chem.* **2017**, *13*, 2131–2137.

(25) Dawson, R.; Laybourn, A.; Clowes, R.; Khimyak, Y. Z.; Adams, D. J.; Cooper, A. I. Functionalized Conjugated Microporous Polymers. *Macromolecules* **2009**, *42*, 8809–8816.

(26) Xie, D.; Yu, D.; Hao, Y.; Han, S.; Li, G.; Wu, X.; Hu, F.; Li, L.; Chen, H. Y.; Liao, Y. F.; Peng, S. Dual-Active Sites Engineering of N-Doped Hollow Carbon Nanocubes Confining Bimetal Alloys as Bifunctional Oxygen Electrocatalysts for Flexible Metal-Air Batteries. *Small* **2021**, *17*, 2007239.

(27) Zhang, S.; Xue, H.; Li, W. L.; Sun, J.; Guo, N.; Song, T.; Dong, H.; Zhang, J.; Ge, X.; Zhang, W.; Wang, Q. Constructing Precise Coordination of Nickel Active Sites on Hierarchical Porous Carbon Framework for Superior Oxygen Reduction. *Small* **2021**, *17*, 2102125.

(28) Yang, Y.; Dai, Q.; Shi, L.; Liu, Y.; Isimjan, T. T.; Yang, X. Electronic Modulation of Pt Nanoparticles on Ni₃N-Mo₂C by Support-Induced Strategy for Accelerating Hydrogen Oxidation and Evolution. *J. Phys. Chem. Lett.* **2022**, *13*, 2107–2116.

(29) Wang, Y.; Zheng, M.; Sun, H.; Zhang, X.; Luan, C.; Li, Y.; Zhao, L.; Zhao, H.; Dai, X.; Ye, J.-Y.; Wang, H.; Sun, S.-G. Catalytic Ru containing Pt₃Mn nanocrystals enclosed with high-indexed facets: Surface alloyed Ru makes Pt more active than Ru particles for ethylene glycol oxidation. *Appl. Catal. B Environ.* **2019**, *253*, 11–20.

(30) Qi, Y.; Chai, N.; Gu, Q.; Chen, J.; Lu, M.; Zhang, X.; Zhang, B. Catalytic polysulfide conversion in lithium-sulfur batteries by platinum nanoparticles supported on carbonized microspheres. *Chem. Eng. J.* **2022**, *435*, 135112.

(31) Hu, Y.; Luo, Z.; Guo, M.; Dong, J.; Yan, P.; Hu, C.; Isimjan, T. T.; Yang, X. Interface engineering of Co₂N_{0.67}/CoMoO₄ heterostructure nanosheets as a highly active electrocatalyst for overall water splitting and Zn-H₂O cell. *Chem. Eng. J.* **2022**, *435*, 134795.

(32) Yang, G.; Jiao, Y.; Yan, H.; Xie, Y.; Wu, A.; Dong, X.; Guo, D.; Tian, C.; Fu, H. Interfacial Engineering of MoO₂-FeP Heterojunction for Highly Efficient Hydrogen Evolution Coupled with Biomass Electrooxidation. *Adv. Mater.* **2020**, *32*, 2000455.

(33) Geng, B.; Yan, F.; Liu, L.; Zhu, C.; Li, B.; Chen, Y. Ni/MoC heteronanoparticles encapsulated within nitrogen-doped carbon nanotube arrays as highly efficient self-supported electrodes for overall water splitting. *Chem. Eng. J.* **2021**, *406*, 126815.

(34) Liu, J.; Wang, J.; Fo, Y.; Zhang, B.; Molochas, C.; Gao, J.; Li, W.; Cui, X.; Zhou, X.; Jiang, L.; Tsiakaras, P. Engineering of unique Ni-Ru nano-twins for highly active and robust bifunctional hydrogen oxidation and hydrogen evolution electrocatalysis. *Chem. Eng. J.* **2023**, *454*, 139959.

(35) Sheng, W.; Zhuang, Z.; Gao, M.; Zheng, J.; Chen, J. G.; Yan, Y. Correlating hydrogen oxidation and evolution activity on platinum at

different pH with measured hydrogen binding energy. *Nat. Commun.* **2015**, *6*, 5848.

(36) Qin, B.; Yu, H.; Gao, X.; Yao, D.; Sun, X.; Song, W.; Yi, B.; Shao, Z. Ultrathin IrRu nanowire networks with high performance and durability for the hydrogen oxidation reaction in alkaline anion exchange membrane fuel cells. *J. Mater. Chem. A* **2018**, *6*, 20374–20382.

(37) Zhang, J.; Qu, X.; Shen, L.; Li, G.; Zhang, T.; Zheng, J.; Ji, L.; Yan, W.; Han, Y.; Cheng, X.; Jiang, Y.; Sun, S. Engineering the Near-Surface of PtRu₃ Nanoparticles to Improve Hydrogen Oxidation Activity in Alkaline Electrolyte. *Small* **2021**, *17*, 2006698.

(38) Li, C.; Jang, H.; Liu, S. G.; Kim, M. G.; Hou, L. Q.; Liu, X. E.; Cho, J. P and Mo Dual Doped Ru Ultrasmall Nanoclusters Embedded in P-Doped Porous Carbon toward Efficient Hydrogen Evolution Reaction. *Adv. Energy Mater.* **2022**, *12*, 2200029.

(39) Yang, F.; Bao, X.; Li, P.; Wang, X.; Cheng, G.; Chen, S.; Luo, W. Boosting Hydrogen Oxidation Activity of Ni in Alkaline Media through Oxygen-Vacancy-Rich CeO₂/Ni Heterostructures. *Angew. Chem., Int. Ed.* **2019**, *58*, 14179–14183.

(40) Li, L.; Liu, S.; Zhan, C.; Wen, Y.; Sun, Z.; Han, J.; Chan, T.-S.; Zhang, Q.; Hu, Z.; Huang, X. Surface and Lattice Engineered Ruthenium Superstructures towards High-Performance Bifunctional Hydrogen Catalysis. *Energy Environ. Sci.* **2023**, *16*, 157–166.

(41) Yang, Y.; Zhao, L.; Sun, Y.; Lin, Y.; Yang, L.; Mao, K.; Li, C.; Xu, K. Tuning Electron Transfer in Atomic-Scale Pt-Supported Catalysts for the Alkaline Hydrogen Oxidation Reaction. *Inorg. Chem.* **2023**, *62*, 5032–5039.

(42) Lyu, S.; Guo, C.; Wang, J.; Li, Z.; Yang, B.; Lei, L.; Wang, L.; Xiao, J.; Zhang, T.; Hou, Y. Exceptional catalytic activity of oxygen evolution reaction via two-dimensional graphene multilayer confined metal-organic frameworks. *Nat. Commun.* **2022**, *13*, 6171.

(43) Mao, J.; He, C. T.; Pei, J.; Chen, W.; He, D.; He, Y.; Zhuang, Z.; Chen, C.; Peng, Q.; Wang, D.; Li, Y. Accelerating water dissociation kinetics by isolating cobalt atoms into ruthenium lattice. *Nat. Commun.* **2018**, *9*, 4958.

(44) Zhang, J.; Li, Z.; Chen, Y.; Gao, S.; Lou, X. W. D. Nickel-Iron Layered Double Hydroxide Hollow Polyhedrons as a Superior Sulfur Host for Lithium-Sulfur Batteries. *Angew. Chem., Int. Ed.* **2018**, *57*, 10944–10948.

(45) Wang, T.; Wang, P.; Zang, W.; Li, X.; Chen, D.; Kou, Z.; Mu, S.; Wang, J. Nanoframes of Co₃O₄-Mo₂N Heterointerfaces Enable High-Performance Bifunctionality toward Both Electrocatalytic HER and OER. *Adv. Funct. Mater.* **2022**, *32*, 2107382.

(46) Jiao, S.; Fu, X.; Wang, S.; Zhao, Y. Perfecting electrocatalysts via imperfections: towards the large-scale deployment of water electrolysis technology. *Energy Environ. Sci.* **2021**, *14*, 1722–1770.

(47) Tan, F.; Zhou, Y.; Zhang, H.; Sun, P.; Li, H.; Liu, X.; Wågberg, T.; Hu, G. Improving the hydrogen evolution reaction activity of molybdenum-based heterojunction nanocluster capsules via electronic modulation by erbium-nitrogen-phosphorus ternary doping. *Chem. Eng. J.* **2023**, *454*, 140079.

(48) Li, J.; Ghoshal, S.; Bates, M. K.; Miller, T. E.; Davies, V.; Stavitski, E.; Attenkofer, K.; Mukerjee, S.; Ma, Z. F.; Jia, Q. Experimental Proof of the Bifunctional Mechanism for the Hydrogen Oxidation in Alkaline Media. *Angew. Chem., Int. Ed.* **2017**, *56*, 15594–15598.

(49) Li, H.; Liu, K.; Fu, J.; Chen, K.; Yang, K.; Lin, Y.; Yang, B.; Wang, Q.; Pan, H.; Cai, Z.; Li, H.; Cao, M.; Hu, J.; Lu, Y.-R.; Chan, T.-S.; Cortés, E.; Fratallocchi, A.; Liu, M. Paired Ru-O-Mo ensemble for efficient and stable alkaline hydrogen evolution reaction. *Nano Energy* **2021**, *82*, 105767.

(50) Jiang, X.; Jang, H.; Liu, S.; Li, Z.; Kim, M. G.; Li, C.; Qin, Q.; Liu, X.; Cho, J. The Heterostructure of Ru₂P/WO₃/NPC Synergistically Promotes H₂O Dissociation for Improved Hydrogen Evolution. *Angew. Chem., Int. Ed.* **2021**, *60*, 4110–4116.

(51) Xiong, B.; Jin, B.; Zhao, W.; Zhou, H.; Luo, J.; Si, D.; Chen, L.; Shi, J. NiMo Nanoparticles Anchored on N-Doped Carbon Rods for High-Efficiency Hydrogen Electrooxidation in Alkaline Media. *ACS Appl. Mater. Interfaces* **2021**, *13*, 15475–15481.

(52) Guo, M.; Xu, M.; Qu, Y.; Hu, C.; Yan, P.; Isimjan, T. T.; Yang, X. Electronic/mass transport increased hollow porous Cu₃P/MoP nanospheres with strong electronic interaction for promoting oxygen reduction in Zn-air batteries. *Appl. Catal. B: Environ.* **2021**, *297*, 120415.

Recommended by ACS

Tunable Pt–Ni Interaction Induced Construction of Disparate Atomically Dispersed Pt Sites for Acidic Hydrogen Evolution

Yidan Peng, Yang Li, *et al.*

MAY 24, 2023

ACS APPLIED MATERIALS & INTERFACES

READ 

Unveiling the Adsorption Behavior and Redox Properties of PtNi Nanowire for Biomass-Derived Molecules Electrooxidation

Jingcheng Wu, Yuqin Zou, *et al.*

DECEMBER 07, 2022

ACS NANO

READ 

Recent Advances and Perspectives in Ru Hybrid Electrocatalysts for the Hydrogen Evolution Reaction

Yiwen Li and Ligang Feng

MAY 26, 2023

ENERGY & FUELS

READ 

Bimetallic PtNi Nanoclusters Supported on Carbon Nanospheres as Catalysts for H₂ Production from Dimethylamineborane Hydrolysis

Wenkai Huang, Xiang Liu, *et al.*

NOVEMBER 29, 2022

ACS APPLIED NANO MATERIALS

READ 

Get More Suggestions >